



Synthesis of silica@C-dots/phosphotungstates core-shell microsphere for effective oxidative-adsorptive desulfurization of dibenzothiophene with less oxidant



Yongqiang Zhang, Rui Wang*

School of Environmental Science and Engineering, Shandong University, No. 27 Shanda South Road, Jinan 250199, PR China

ARTICLE INFO

Keywords:
Core-Shell microsphere
Oxidative-adsorptive desulfurization
Phosphotungstates calcination
Carbon dots
Cocatalyst

ABSTRACT

A core-shell microsphere catalyst with a solid silica core and a mesoporous shell made up of quaternary ammonium phosphotungstate and carbon dots (C-dots) was successfully synthesized for the oxidative-adsorptive desulfurization (ODS) of dibenzothiophene (DBT) in fuel oil. The phosphotungstic acid used for the synthesis of the catalyst was calcined to enhance its activity. XRD, FT-IR and catalytic test showed that the defective Keggin anion $[PW_{12}O_{38}]^{3-}$ formed under proper calcination conditions could explain the activity enhancement. EPR measurement indicated that hydroxyl radicals were generated from H_2O_2 by the interaction with C-dots, which proved C-dots to be an efficient cocatalyst in the system. The synergistic effect of $[PW_{12}O_{38}]^{3-}$ and C-dots in the synthesized catalyst remarkably improve the utilization efficiency of H_2O_2 . When the loading amount of phosphotungstate and C-dots were optimized to 25% and 0.45%, the ODS system showed best desulfurization capacity under 50 °C. A high ODS efficiency of 98.08% could still be achieved even when the ratio of $n(H_2O_2)/n(DBT)$ was reduced to 1.75. The existence of dibenzothiophene sulfoxide (DBTO) in the acetonitrile eluent of spent catalyst was confirmed by LC-MS spectra. The characterization results indicated that part of the DBT was oxidized to its corresponding sulfoxide which need less oxidant than sulfone. Both of the oxidation products could be eliminated from oil phase by adsorption on the catalyst.

1. Introduction

In spite of the increasing concerns on renewables during the last decades, natural fossil fuels such as natural gas, coal and crude oil still dominate energy sources in the world. It is a matter of fact that crude oil remains feed stocks of various industrial departments powering national economy in developed and developing countries. However, sulfur organic compounds existing in crude oil and its distillation products are big threats for environment because of the harmful SO_x derivatives emission from their combustion [1,2]. Especially, with the growing number of automobiles around the world, desulfurization of all kinds of transportation fuel oils has attracted much more concerns from global governments and researchers. Nowadays, the level of sulfur content in fuel oils has been strictly limited to less than 10 ppm in many countries, which means efficient and low-cost desulfurization techniques in refinery industry are quite necessary [3–6]. The mainly used traditional hydrodesulfurization (HDS) process is a high effective desulfurization method for aliphatic and acyclic S-compound under high temperature (300–400 °C) and pressure (20–100 atm of H_2). But HDS has difficulty to remove the refractory aromatic sulfur compounds such

as dibenzothiophene (DBT) and its derivatives unless the operation temperature and pressure were further elevated, which means more cost investment [7,8]. So, alternative desulfurization routes have been investigated in recent decade. Among them, oxidative desulfurization (ODS) has attracted considerable interest due to its high efficiency for the removal of refractory sulfur compounds under mild reaction conditions.

The choice of catalyst and oxidant is vital to the desulfurization effect in ODS process. Polyoxometalates (POMs) catalysts have been widely used in the oxidation of many organic substrates for its high activity, environmental benignity and tunable characteristics [9–11]. Although a variety of POMs catalysts were synthesized and applied in the oxidation of DBT and its derivatives in fuel oil, the application potential of these catalysts are greatly hindered by their high solubility in polar solvent and low specific surface area, which will influence the recyclability and catalytic activity of POM catalysts, respectively [12–14]. To overcome the drawbacks, POMs were immobilized on porous materials such as zeolite molecular sieve [15], metal-organic frameworks (MOFs) [12,17], mesoporous silica [16], ion exchange resin [18] or carbon materials [19] to form heterogeneous catalysts.

* Corresponding author.

E-mail address: wangrui@sdu.edu.cn (R. Wang).

Nevertheless, there still exist some problems of the synthesized heterogeneous catalysts including weak interaction between the active species and porous materials, and lower degree of exposure of catalytic sites in organic phase compared to homogeneous catalysts. It has been reported that hydrophobization of porous support by hydrophobic organic group could significantly improve the stability of POMs active sites and activity of the composite catalyst [15,20,21]. Inspired by the literatures, a core-shell microsphere aggregation structure containing silica and quaternary ammonium phosphotungstate was manufactured in our work. The amphiphilic phosphotungstate containing quaternary ammonium cation was employed both as hydrophobic modification and active component in the synthesized catalyst. Unlike the common supported mesoporous materials in which the active component was immobilized in the pores or channels of the carrier [22–24], amphiphilic phosphotungstate appeared on the external surface of silica core forming a solid shell here.

Hydrogen peroxide (H_2O_2) was a classic oxidant in ODS process due to its green resultant (water only) and high reactivity [25]. But on account of the non-productive decomposition of H_2O_2 to O_2 and water, excess amount of H_2O_2 (3–10 equivalents to the substrates) was commonly needed to obtain high conversion of refractory sulfur compound, which lead to more ODS cost [26–28]. Therefore, developing highly-active catalysts and systems to scant the invalid decomposition and decrease the dosage of H_2O_2 is very important for the industrial application of ODS [29,30]. Carbon dots (C-dots) have been attracting attention as a novel nanocarbon material in recent years. With unique photo-generated electron transfer/reservoir properties, abundant functional groups and small size, it often acts as an efficient component distributed in photocatalysts uniformly [31–33]. But, despite the extensive use of various nanocarbon materials as metal-free catalysts in thermal catalysis reactions [34], the thermal catalytic properties of C-dots are rarely reported. Here, C-dots were employed as a catalytic promoter in the composite catalyst to improve the utilization efficiency of H_2O_2 through supplying one more route for its productive utilization.

In this paper, the catalytic activity of $H_3PW_{12}O_{40} \cdot xH_2O$ (HPW) was enhanced by pretreatment of calcination at proper conditions in the beginning. The relation between ODS performance of thermal treated HPW and calcination conditions was revealed and the possible mechanism was discussed. Then the treated HPW with higher activity was used to prepare amphiphilic phosphotungstate with stearyl trimethyl ammonium bromide (STAB). The $SiO_2@C$ -dots/phosphotungstate catalyst with an inert SiO_2 core and a catalytic active shell made up of the prepared amphiphilic phosphotungstate and C-dots was synthesized through sol-gel method combined with freeze-drying. The synthesized $SiO_2@C$ -dots/phosphotungstate catalyst was used as both catalyst and mesoporous adsorbent simultaneously in the oxidative-adsorptive desulfurization (OADS) system. DBT was oxidized to corresponding sulf oxide and sulfone with greater polarity and removed from the oil phase by adsorption on the catalyst in OADS process. High desulfurization efficiency of 98.08% was accomplished with H_2O_2 less than 2 equivalents to DBT in the absence of any extraction agent. The mechanisms of the catalysis reaction were investigated and discussed on the basis of controlled experiments and different characterization methods.

2. Experimental

2.1. Preparation of C-dots solution

All chemicals used in these experiments are analytical reagent grade and commercial available. C-dots solution was manufactured through a typical electrochemical method reported in literature [33]. Two graphite rods were put in 800 ml ultrapure water in parallel with the separation distance about 7 cm as anode and cathode, respectively. Static voltage of 30 V was applied on the electrodes by a direct current supply. After being stirred continuously for 120 h, the formed dark-yellow solution was filtered with 0.22 μ m filter membrane to remove the

insoluble graphite particles and C-dots powder can be obtained by freeze drying the filtrate.

2.2. Calcination treatment of phosphotungstic acid

Commercial HPW (2 g) was heated up to certain temperature in a 100 ml covered crucible and maintained at this temperature for different times. Samples of HPW calcined at different temperatures for 1 h (250 °C, 350 °C, 450 °C, 550 °C, 650 °C denoted as PW2501, PW3501, PW4501, PW5501, PW6501 separately) and samples of HPW calcined at 550 °C for different times (1 h, 2 h, 3 h, 4 h, 5 h denoted as PW5501, PW5502, PW5503, PW5504, PW5505 respectively) were prepared for comparision.

2.3. Preparation of amphiphilic phosphotungstates and $SiO_2@C$ -dots/phosphotungstate core-shell microsphere aggregation

To synthesize the amphiphilic phosphotungstates, the prepared PW5501 and STAB were dissolved in deionized water respectively with the help of ultrasound method, and then, the two solutions were mixed and stirred for 2 h. After that, the white particiate was separated from the mixed solution by vacuum suction filtration and washed with deionized water to remove redundant bromide ions. Then, the product was dried at 80 °C overnight to obtain amphiphilic phosphotungstates denoted as QPW5501. In the synthesis of $SiO_2@C$ -dots/phosphotungstate, 6 ml tetraethyl orthosilicate (TEOS) was dissolved in 6 ml ethanol, and 50 ml H_2O and 1.5 ml NH_3H_2O was added into the solution. After that, the solution was vigorously stirred for 2 h. Then, QPW5501 dissolved in ethanol along with certain amount of C-dots solution was added in the mixed solution and stirred for another 4 h. Finally, the gray paste was filtrated from the mixture and freeze-dried to gray powder which was labeled as $SiO_2@C$ -dots/QPW5501.

2.4. Characterization

X-ray diffraction (XRD) patterns were collected by Bruker D8 ADVANCE instrument using Cu-K α radiation ($\lambda = 0.15405$ nm, 40 KV \times 60 mA) from 8 ° to 80 ° (20) with the scanning rate of 15 °/min. Fourier Transform Infrared (FT-IR) spectra of the samples were recorded by Bruker ALPHA-T Fourier Transform Infrared Spectrometer, with a range of 400–4000 cm^{-1} using KBr pellet at room temperature. The Raman spectrum was obtained using a HORIBA LabRAM HR800 Raman microscope by a 473 nm laser source. ^{31}P NMR spectra were collected on a Bruker ADVANVE 400 MHZ NMR spectrometer. The nitrogen adsorption–desorption isotherms of the composite catalyst at 77 K were investigated using an Autosorb-IQ surface area and porosity analyzer (Quantachrome Instrument Corp.). The morphologies of the samples were performed on a JSM-6700F cold field emission scanning electron microscope (SEM) (JEOL Ltd.) equipped with an Oxford INCA X sight energy spectrum analyzer using the acceleration voltage of 2 kV. Transition electron microscopy (TEM) images were acquired on a JEM-2100 microscope (JEL Ltd.) using the acceleration voltage of 200 kV. Electron paramagnetic resonance (EPR) signals of radicals trapped by DMPO were recorded on a JES FA200 (JEOL Ltd.) spectrometer.

2.5. Catalytic test and OADS experiment in simulated oil

Catalytic tests of calcined HPW at different conditions and prepared amphiphilic phosphotungstates were conducted in simulated oil of n-octane containing DBT with sulfur content of 50 ppm and 250 ppm, respectively. In a typical run, 60 ml simulated oil was added to a 250 ml three necked flask and warmed up to corresponding temperature, then catalysts and 30 wt % H_2O_2 was added into the mixture with continuous magnetic stirring. Because of the poor adsorptive ability of treated HPW and prepared amphiphilic phosphotungstates, 60 ml of acetonitrile was also added in the reaction system as extraction agent to perform

simultaneous extraction along the reaction time. The solution was stirred for 3 h and the upper layer was sampled in different time intervals.

OADS experiment was conducted similarly as follows: 60 ml simulated oil containing DBT with sulfur content of 250 ppm was added to a 250 ml three necked flask and heated up to 60 °C. Then, 0.2 g SiO₂@C-dots/QPW5501 and corresponding amount of 30 wt % H₂O₂ were added into the mixture with continuous stirring. The DBT concentrations in model oil after reaction was analyzed by a total sulfur analyzer (WK-2E microcoulometer).

DBT and its oxidized products were also characterized by Gas Chromatography-Mass Spectrometer (GC-MS) (Agilent 6890-Gas Chromatography (GC)/Mass Selective Detector (MSD); HP-5 MS column, 30 m × 250 μm i.d. × 0.25 μm; temperature program: 100 °C temperature rising 10 °C/min–280 °C for 18 min) and High Performance Liquid Chromatography- Mass Spectrometer (HPLC-MS) (Thermo Ultimate 3000 High Performance Liquid Chromatography equipped with a Thermo LCQ Fleet Mass Detector).

3. Results and discussion

3.1. Calcination treatment of HPW

3.1.1. Characterization of calcined HPW

XRD patterns of HPW samples calcined at different temperatures for

1 h are shown in Fig. 1(a). Characteristic diffraction peaks of H₃PW₁₂O₄₀ (JCPDS 50-0657) at $2\theta = 10.3^\circ, 20.7^\circ, 23.1^\circ, 25.4^\circ$, and 29.5° were clearly detected when the calcination temperature was from 250 °C to 450 °C, indicating that the keggin structure of phosphotungstic anion was intact in this temperature range. When the sample was calcined at 550 °C for 1 h (PW5501), diffraction peaks of H₃PW₁₂O₄₀ vanished and new diffraction peaks appeared at $2\theta = 17.3^\circ, 24.6^\circ$ and 28.9° . These peaks can be assigned to “denuded” Keggin anion [PW₁₂O₃₈]³⁻ (JCPDS 50-0658), which was an oxygen defective phase transformed from [PW₁₂O₄₀]³⁻ by loss of two oxygen atoms in the Keggin structure [35]. And after being treated for 1 h at 650 °C, the distinct diffraction peaks of WO₃ (JCPDS 46-1096) located at $2\theta = 23.62^\circ$ and 33.6° demonstrated that the Keggin's framework was completely destroyed. The detailed transformation process from [PW₁₂O₃₈]³⁻ to WO₃ could be analyzed through the XRD patterns in Fig. 1(b). The nearly unchanged diffraction spectra of the first two hours under 550 °C demonstrated that the intermediate phase [PW₁₂O₃₈]³⁻ possess good thermal stability as a stable solid catalyst. And then characteristic diffraction peaks of WO₃ at $2\theta = 23.62^\circ$ and 33.6° showed up and grew more obvious when the calcination time extended from 3 h to 4 h which could give the evidence that the [PW₁₂O₃₈]³⁻ phase was destroyed gradually. When the treated time reached 6 h, all Keggin structures in the sample were decomposed to WO₃ completely as shown in Fig. 1(b). XRD patterns of PW5501 before and after reaction are compared in Fig. 1(c). It can be seen that the

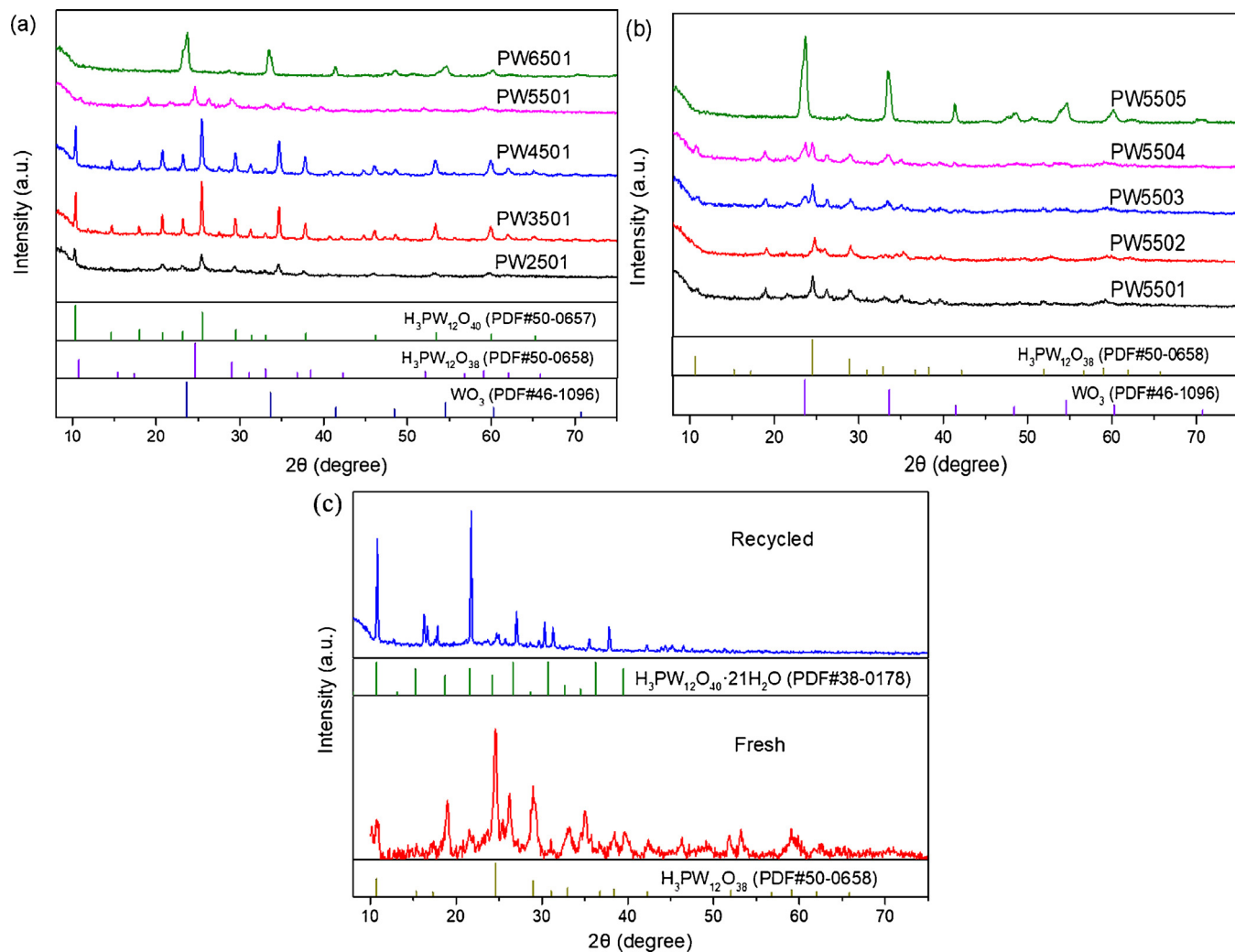


Fig. 1. XRD spectra collected from HPW samples calcined at different conditions. (a) HPW calcined at different temperatures from 250 °C to 650 °C for 1 h. (b) HPW calcined at 550 °C for different time from 1 h to 5 h. (c) XRD spectra of PW5501 before and after oxidation reaction.

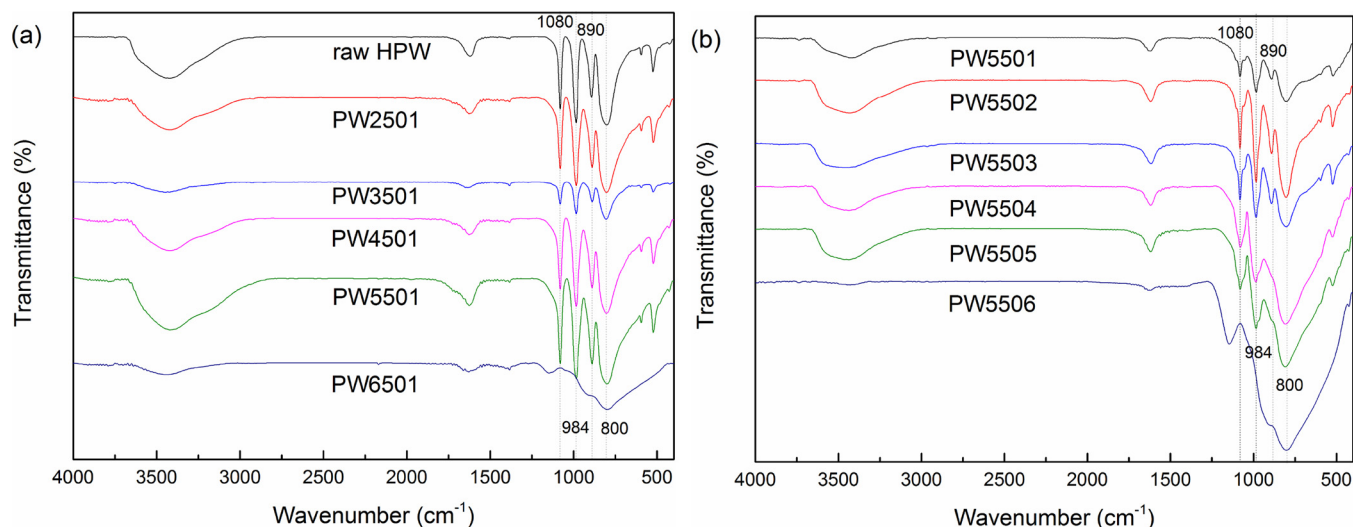


Fig. 2. FT-IR spectra of HPW samples calcined at different conditions. (a) HPW calcined at different temperatures from 250 °C to 650 °C for 1 h. (b) HPW calcined at 550 °C for different time from 1 h to 6 h.

characteristic peaks of $[\text{PW}_{12}\text{O}_{38}]^{3-}$ at $2\theta = 10.7^\circ, 17.3^\circ, 24.6^\circ$ and 28.9° disappeared after PW5501 was recycled. The intensive peaks shown at $2\theta = 10.7^\circ, 21.6$ and 26.6 can be assigned to the hydrate of phosphotungstic acid $\text{H}_3\text{PW}_{12}\text{O}_{40}\cdot12\text{H}_2\text{O}$. That indicates that the $[\text{PW}_{12}\text{O}_{38}]^{3-}$ formed by calcination process was oxidized back to $[\text{PW}_{12}\text{O}_{40}]^{3-}$ after the oxidative reaction.

Fig. 2 shows the FT-IR spectra of HPW calcined at different conditions. The four strong FT-IR peaks appeared at 1080 cm^{-1} ($\text{P}-\text{O}$), 984 cm^{-1} ($\text{W}=\text{O}$), 890 cm^{-1} ($\text{W}-\text{O}_b-\text{W}$) and 800 cm^{-1} ($\text{W}-\text{O}_c-\text{W}$) are typical bands of HPW with Keggin structure [36]. It could be seen in Fig. 2 (a) that all the typical peaks of Keggin structure in HPW could still be found in PW5501 which was identified as defective phase $[\text{PW}_{12}\text{O}_{38}]^{3-}$ in the analysis of XRD patterns above. This indicates that, despite the loss of about one water molecular, the stable Keggin structure was maintained in $[\text{PW}_{12}\text{O}_{38}]^{3-}$ with oxygen defects. The Keggin structure was decomposed to WO_3 completely according to the wide single peak at 800 cm^{-1} showed in PW5506 [37]. As shown in Fig. 2(b), starting at 4 h, the $\text{W}-\text{O}_b-\text{W}$ peak at 890 cm^{-1} disappeared and the $\text{W}-\text{O}_c-\text{W}$ peak at 800 cm^{-1} became broader, which means the collapse of Keggin structure occurred. And after treated for six hours at 550°C , all typical peaks of Keggin structure vanished except for the band of $\text{W}-\text{O}$ at 800 cm^{-1} indicating the samples were transformed to WO_3 completely, which is consistent with the XRD results.

3.1.2. Catalytic test of calcined HPW samples

The catalytic activity of calcined samples were evaluated in ODS process with H_2O_2 as oxidant to investigate the relations between their structures and desulfurization effects. The results of evaluation are presented in Fig. 3. According to our blank experiment, the extraction desulfurization efficiency could only reach 48.45% in the absence of any catalyst and oxidant. As we can see in Fig. 3, sulfur removal was remarkably improved after the catalyst and H_2O_2 were added into the system. And the catalytic activity of calcined samples greatly improved when the calcination temperature rised from 250°C to 550°C . The highest desulfurization efficiency of 98.32% was reached by PW5501 with H_2O_2 as oxidant. Whether to increase the calcination temperature or extend the calcination time will cause a decline in the desulfurization capacity of calcined samples. Turn over frequencies (TOFs) of different calcined HPW samples are calculated and listed in Table 1. TOF = number of transformed DBT per minute/ number of active sites. We approximated the number of active sites by the number of catalyst molecules. It can be seen that the TOFs of PW5501, PW5502 and PW5503 are much higher than that of other samples. Taking the

characterization analysis elaborated in 3.1.1 into consideration, the much higher TOF value can be attributed to the “denuded” Keggin anion $[\text{PW}_{12}\text{O}_{38}]^{3-}$ with oxygen defects formed by proper calcination which possesses much higher catalytic capacity than the raw HPW or the WO_3 obtained by the complete thermal decomposition of HPW. It also can be seen from Table 1 that the calcined HPW samples have very low surface areas and the TOF values of the samples were not influenced by the surface areas. According to the fact that the TOF decreased in the sequence of PW5501 > PW5502 > PW5503 > PW5504 > PW5505, the decline of the catalytic activity can be explained by the XRD analysis that the structure of $[\text{PW}_{12}\text{O}_{38}]^{3-}$ begin to collapse at 550°C when the calcined time exceeds 1 h. The changes on the crystalline structure and desulfurization activity are illustrated in Scheme 1.

To further investigate reason causing the differences on the catalytic oxidation activity of PW5501 and raw HPW, ^{31}P NMR spectra were employed to characterize the two catalysts and their products reacting with H_2O_2 . The results are presented in Fig. 4(A). The identical peaks at 15.2 ppm appeared in the NMR spectra of raw HPW (Fig. 4(A) a) and PW5501 (Fig. 4(A) b) can be assigned to the phosphotungstic Keggin structure of the two catalysts. The peak of peroxoheteropolyanions $\{\text{PO}_4[\text{WO}(\text{O}_2)_2]_4\}^{3-}$ appeared at 12.5 ppm as shown in Fig. 4(A) c. The peroxoheteropolyanions $\{\text{PO}_4[\text{WO}(\text{O}_2)_2]_4\}^{3-}$ used for NMR characterization was prepared by the reaction of raw HPW and excessive amount of H_2O_2 in our experiment. It has been widely reported that the Keggin heteropolyanion of HPW would form $\{\text{PO}_4[\text{WO}(\text{O}_2)_2]_4\}^{3-}$ with H_2O_2 in the oxidation reactions and the Keggin anion is only a precursor of the true catalyst [38,39]. In order to identify the ODS activity of $\{\text{PO}_4[\text{WO}(\text{O}_2)_2]_4\}^{3-}$, desulfurization experiment with $\{\text{PO}_4[\text{WO}(\text{O}_2)_2]_4\}^{3-}$ in the absence of H_2O_2 was carried out in Fig. 4(B). The DBT removal could reach 83.5% when the mole ratio of $\{\text{PO}_4[\text{WO}(\text{O}_2)_2]_4\}^{3-}$ and DBT is 2:1. This gave the evidence on the fact that $\{\text{PO}_4[\text{WO}(\text{O}_2)_2]_4\}^{3-}$ possesses remarkable ODS capacity. Therefore, the ability to generate $\{\text{PO}_4[\text{WO}(\text{O}_2)_2]_4\}^{3-}$ with H_2O_2 is crucial to the catalytic capacity of the catalysts. Because of this, the products of PW5501 and raw HPW reacting with equimolar H_2O_2 were detected by ^{31}P NMR in Fig. 4(A) d and Fig. 4(A) e, respectively. The existence of two peaks at 12.5 and 15.2 ppm showed that the Keggin anions in both PW5501 and raw HPW were not transformed to $\{\text{PO}_4[\text{WO}(\text{O}_2)_2]_4\}^{3-}$ completely. However, according to the height of the NMR peaks, the content of $\{\text{PO}_4[\text{WO}(\text{O}_2)_2]_4\}^{3-}$ in PW5501 system was calculated to be 65.43% which is much higher than that of 12.09% in raw HPW system. It is demonstrated that in the system with low H_2O_2 concentration, the defective $[\text{PW}_{12}\text{O}_{38}]^{3-}$ anions in PW5501 are easier to be degraded by H_2O_2 to

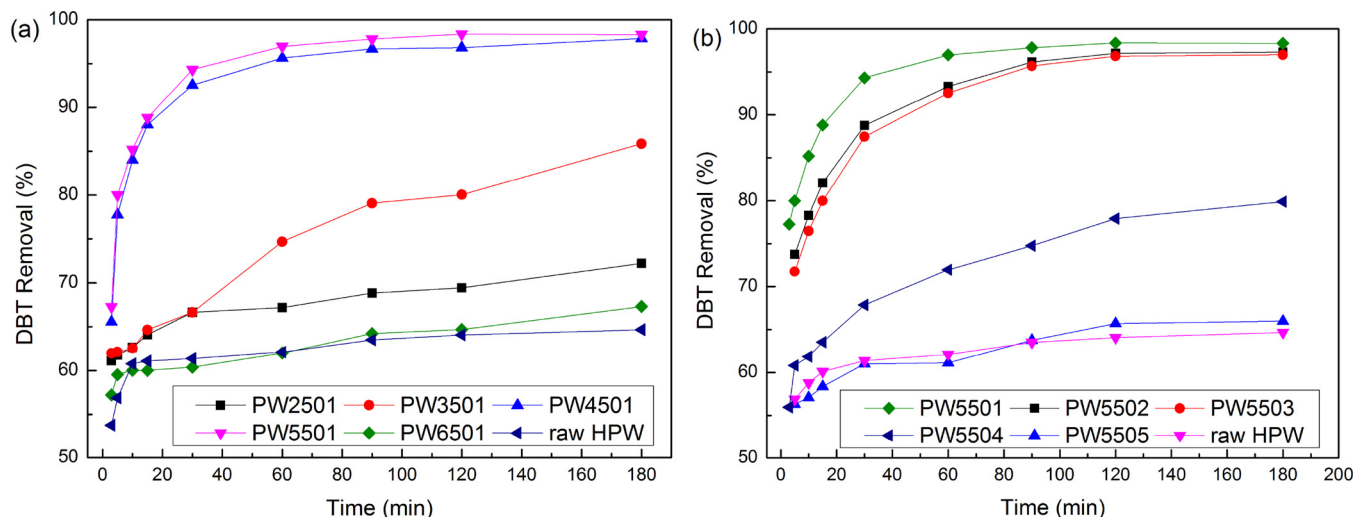


Fig. 3. DBT removal on HPW samples calcined at different conditions. (a) HPW calcined at different temperatures from 250 °C to 650 °C for 1 h. (b) HPW calcined at 550 °C for different time from 1 h to 5 h. Reaction conditions: initial S-content in model oil: 50 ppm; catalyst dosage: 0.05 g; reaction temperature: 60 °C; $n(H_2O_2)/n(DBT) = 5:1$; acetonitrile was used as extraction solvent.

Table 1

Turn over frequencies (TOFs) of different calcined HPW samples in oxidative desulfurization reaction.

Catalysts	Surface area (m^2/g)	TOF ($\text{mol min}^{-1} \text{molecule}_{\text{catalyst}}^{-1}$)
raw HPW	1.3	0.0121
PW2501	1.1	0.0125
PW3501	1.0	0.0269
PW4501	0.7	0.1200
PW5501	0.5	0.1784
PW6501	0.4	0.0113
PW5502	0.4	0.1685
PW5503	0.4	0.1669
PW5504	0.4	0.0215
PW5505	0.4	0.0102

form $\{\text{PO}_4[\text{WO}(\text{O}_2)_2]_4\}^{3-}$ than the complete $[\text{PW}_{12}\text{O}_{40}]^{3-}$ anion of raw HPW. Similar results that the lacunary-type phosphotungstate anion $[\text{PW}_{11}\text{O}_{39}]^{7-}$ owes higher catalytic activity than the complete Keggin-type anion $[\text{PW}_{12}\text{O}_{40}]^{3-}$ were also obtained in Hou's research [40].

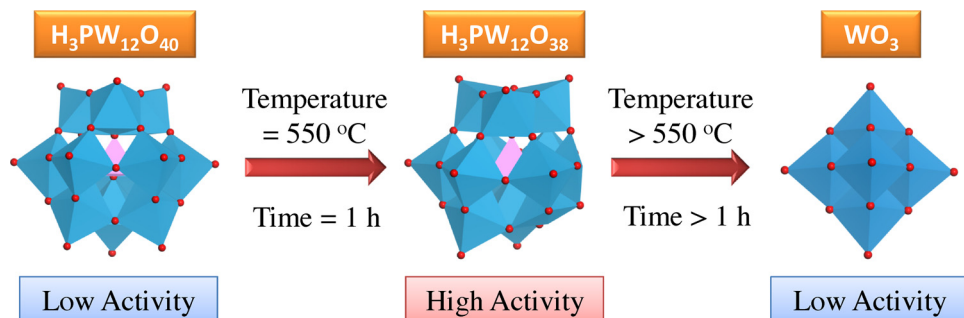
According to **Scheme 1** and ^{31}P NMR characterization, we can see that the key of enhancing the catalytic oxidation activity of HPW by thermal treatment is the extent of calcination. On one hand, proper calcination was needed to get as much $[\text{PW}_{12}\text{O}_{38}]^{3-}$ as we could in the treated samples. On the other hand, excessive calcination must be avoided to decrease the destruction of the Keggin structure and the formation of WO_3 with lower activity. On the basis of our experiments results, PW5501 was chosen for the next synthesis procedure.

3.2. Characterization of synthesized $\text{SiO}_2@\text{C-dots}/\text{QPW5501}$

The amphiphilic phosphotungstate QPW5501 prepared by STAB and PW5501 is characterized by FT-IR spectrum in **Fig. 5**. The bands at 808, 894, 978 and 1079 cm^{-1} are attributed to the Keggin structure of PW5501. The other peaks at 1471, 2852, 2922 and 3030 cm^{-1} belong to the vibration of quaternary ammonium cations of STAB [13]. The FT-IR spectra indicate the successful synthesis of QPW5501.

Fig. 6 shows the N_2 adsorption-desorption isotherms of synthesized catalyst $\text{SiO}_2@\text{C-dots}/\text{QPW5501}$. It could be seen that the isotherms exhibited a typical type-IV curve with a hysteresis loop. The steep increase under relatively pressure (P/P_0) between 0.75 and 0.95 indicated the presence of mesopore with a large pore size in the catalyst [41]. The pore size distribution derived from the adsorption branch using the BJH method shows that the average pore diameter is about 27.2 nm. And the BET surface area of the catalyst are calculated to be $109.5 \text{ m}^2\text{g}^{-1}$ which are much higher than that of QPW5501 ($0.65 \text{ m}^2\text{g}^{-1}$). The mesoporosity and the large surface area of $\text{SiO}_2@\text{C-dots}/\text{QPW5501}$ make it a potential material which can act as both catalysts for the catalytic oxidation of DBT and adsorbents for the adsorption of oxidized products in OADS process.

In order to investigate the morphology and the distribution of every component in $\text{SiO}_2@\text{C-dots}/\text{QPW5501}$, SEM, TEM and energy dispersive X-ray (EDX) mapping analysis were carried out. From the SEM image in **Fig. 7(a)**, a bunch of microspheres with the diameter vary from 200 nm to 1 μm stack closely to form a microsphere aggregation in the synthesis process. The rough spherical surface which can be seen in **Fig. 7(b)** indicates the abundant porous structure on the microsphere surface. TEM images in **Fig. 7(c)** and (d) shows that every microsphere



Scheme 1. Schematic image of changes on the structure and catalytic oxidation activity in the calcination process of HPW.

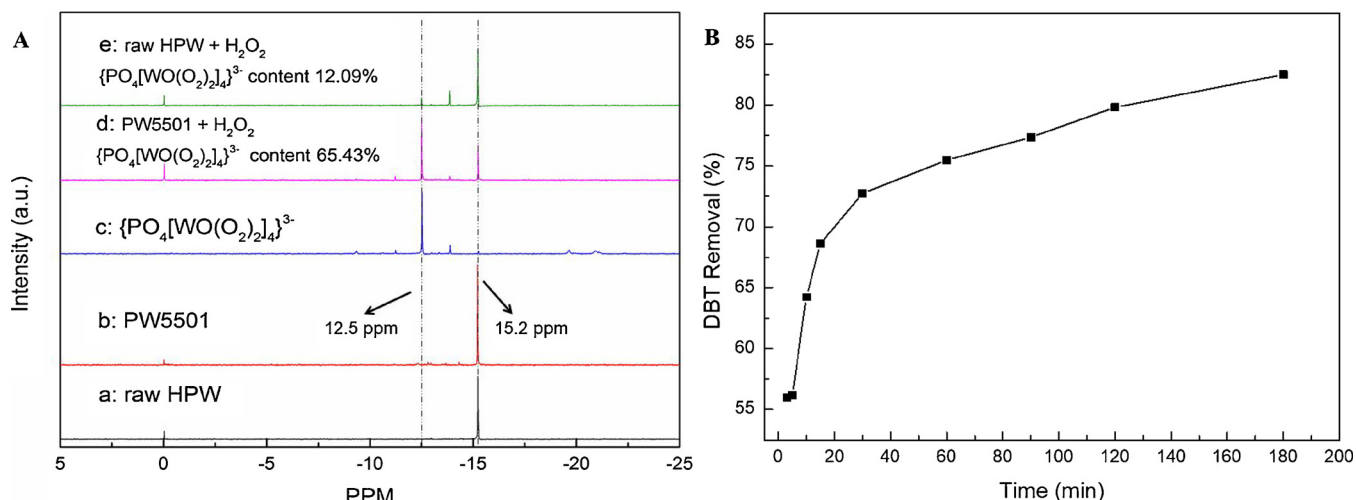


Fig. 4. A: ^{31}P NMR spectra of the phosphotungstic Keggin structure and $\{\text{PO}_4[\text{WO}(\text{O}_2)_2]_4\}^{3-}$ anion in different systems using D_2O as solvent; (a) 0.15 g raw HPW; (b) 0.15 g PW5501; (c) $\{\text{PO}_4[\text{WO}(\text{O}_2)_2]_4\}^{3-}$, $n(\text{HPW})/n(\text{H}_2\text{O}_2) = 1:20$; (d) PW5501 + H_2O_2 , $n(\text{PW5501})/n(\text{H}_2\text{O}_2) = 1:1$; (e) raw HPW + H_2O_2 , $n(\text{raw HPW})/n(\text{H}_2\text{O}_2) = 1:1$. B: Oxidation removal of DBT with $\{\text{PO}_4[\text{WO}(\text{O}_2)_2]_4\}^{3-}$ in the absence of H_2O_2 (initial S-content in model oil: 50 ppm; $n(\{\text{PO}_4[\text{WO}(\text{O}_2)_2]_4\}^{3-}):n(\text{DBT}) = 2:1$; temperature 50 °C).

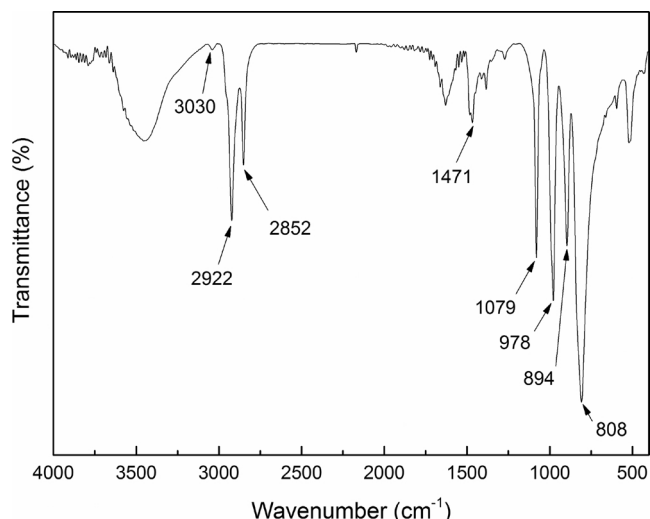


Fig. 5. FT-IR spectra of synthesized amphiphilic phosphotungstates QPW5501.

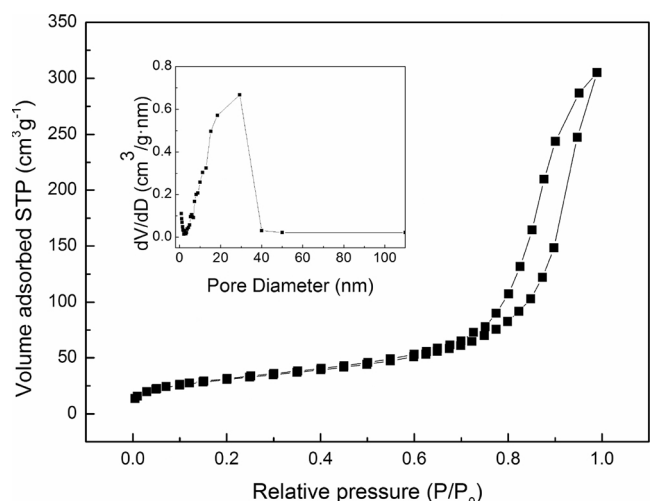


Fig. 6. Nitrogen adsorption–desorption isotherms and BJH pore size distribution curve (inset) of synthesized $\text{SiO}_2@\text{C-dots}/\text{QPW5501}$.

possesses the structure composed of a solid SiO_2 core and a semi-transparent shell with the thickness of dozen nanometers. According to the EDX mapping images in Fig. 8, P and C elements dispersed in consistent with Si spherical skeleton but in a broader space, which demonstrated that QPW5501 and C-dots distribute uniformly in the external shell of SiO_2 core.

3.3. Effects of several parameters on the removal of DBT with H_2O_2

3.3.1. Effects of reaction temperature and the loading of QPW5501

The effect of reaction temperature and loading amount of QPW5501 on the desulfurization efficiency using $\text{SiO}_2@\text{C-dots}/\text{QPW5501}$ catalyst is shown in Fig. 9(a) and (b). It can be seen that reaction temperature of 50 °C was optimum for the catalyst. Through higher temperature would accelerate the reaction to reach a high desulfurization efficiency in a shorter time, the final S removal was hold back due to the more invalid decomposition of H_2O_2 into H_2O and O_2 at high temperature. As the vital active component in $\text{SiO}_2@\text{C-dots}/\text{QPW5501}$, the loading amount of QPW5501 has big influences on the catalytic activity of the catalyst. However, excess loading of QPW5501 might cause a decrease on the adsorptive capacity of the catalyst because of its inherent low surface area. Therefore, in OADS process, loading of QPW5501 was determined to be 25% in the following experiments.

3.3.2. Effect of the loading of C-dots

The dependence of the desulfurization efficiency in the OADS system on the loading of C-dots was investigated under the condition of $n(\text{H}_2\text{O}_2)/n(\text{DBT}) = 1:1$ in Fig. 9(c). The desulfurization efficiency of model fuel on $\text{SiO}_2@\text{C-dots}/\text{QPW5501}$ was obviously improved as the loading amount of C-dots increased from 0 to 0.45%. Comparing to the catalyst without C-dots, nearly a 40% increase on the desulfurization efficiency was achieved when C-dots loading is only 0.45%. After that, the desulfurization efficiency of DBT on the catalyst did not increase continuously with the loading of C-dots. Therefore, the optimized loading of C-dots was determined as 0.45% in the next experiments. In order to find out the influence of C-dots loading on desulfurization rate, the observed data in Fig. 9(c) was fitted to the pseudo first-order reaction equation: $\ln(C/C_0) = -kt$, where the slope parameter k is representative of the rate constant, C_0 is the initial sulfur concentration in model oil, C is the concentration of sulfur compounds in the samples after different reaction time. The reaction constants k under different C-dots loadings are listed in Table 2. We can see that the reaction rate was

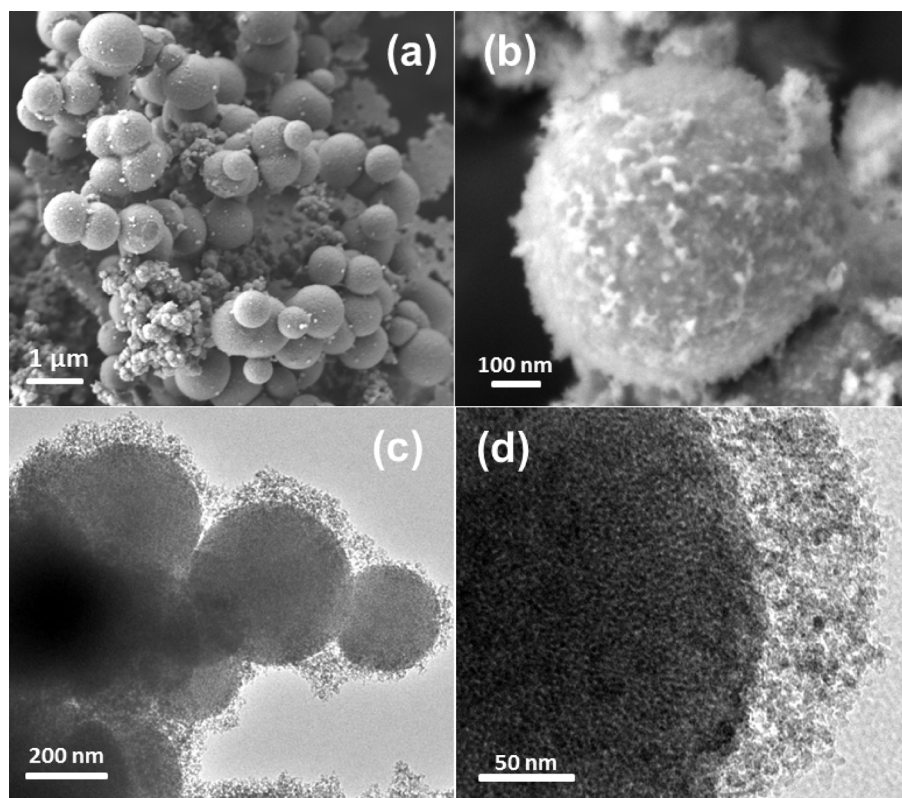


Fig. 7. SEM images (a, b) and TEM images (c, d) of synthesized $\text{SiO}_2@\text{C-dots}/\text{QPW5501}$.

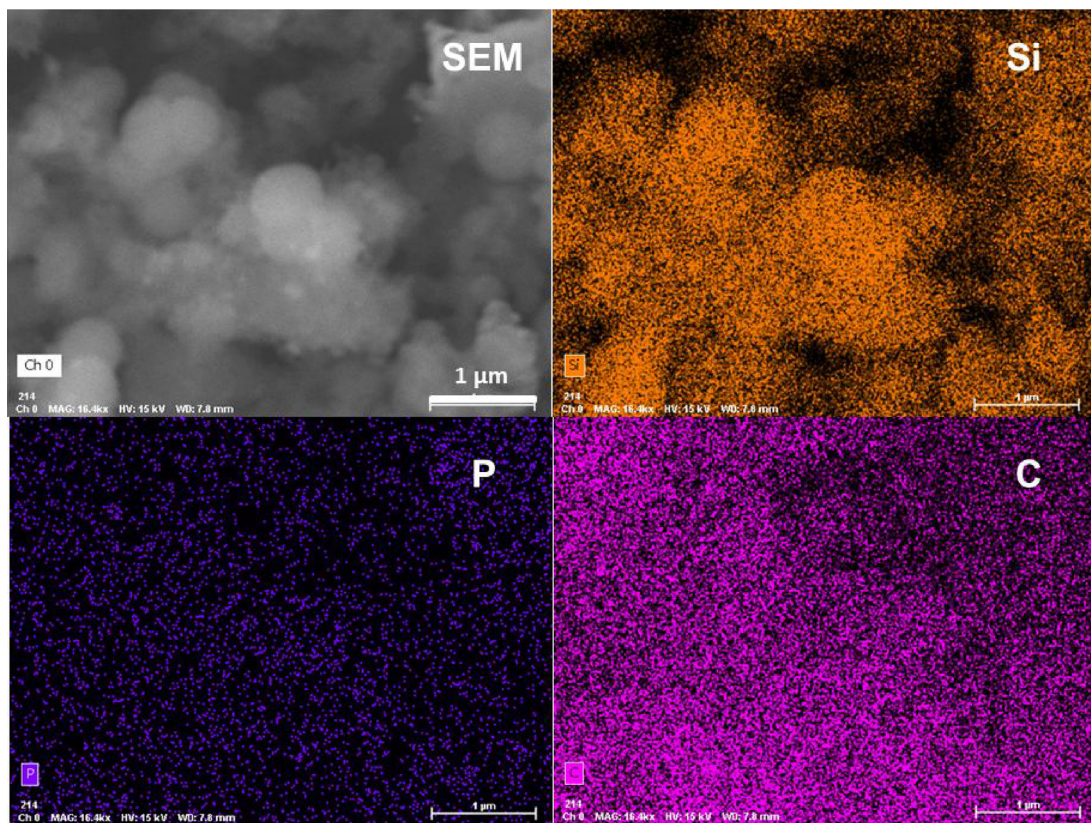


Fig. 8. EDX mapping images of Si, P, and C elements on synthesized $\text{SiO}_2@\text{C-dots}/\text{QPW5501}$.

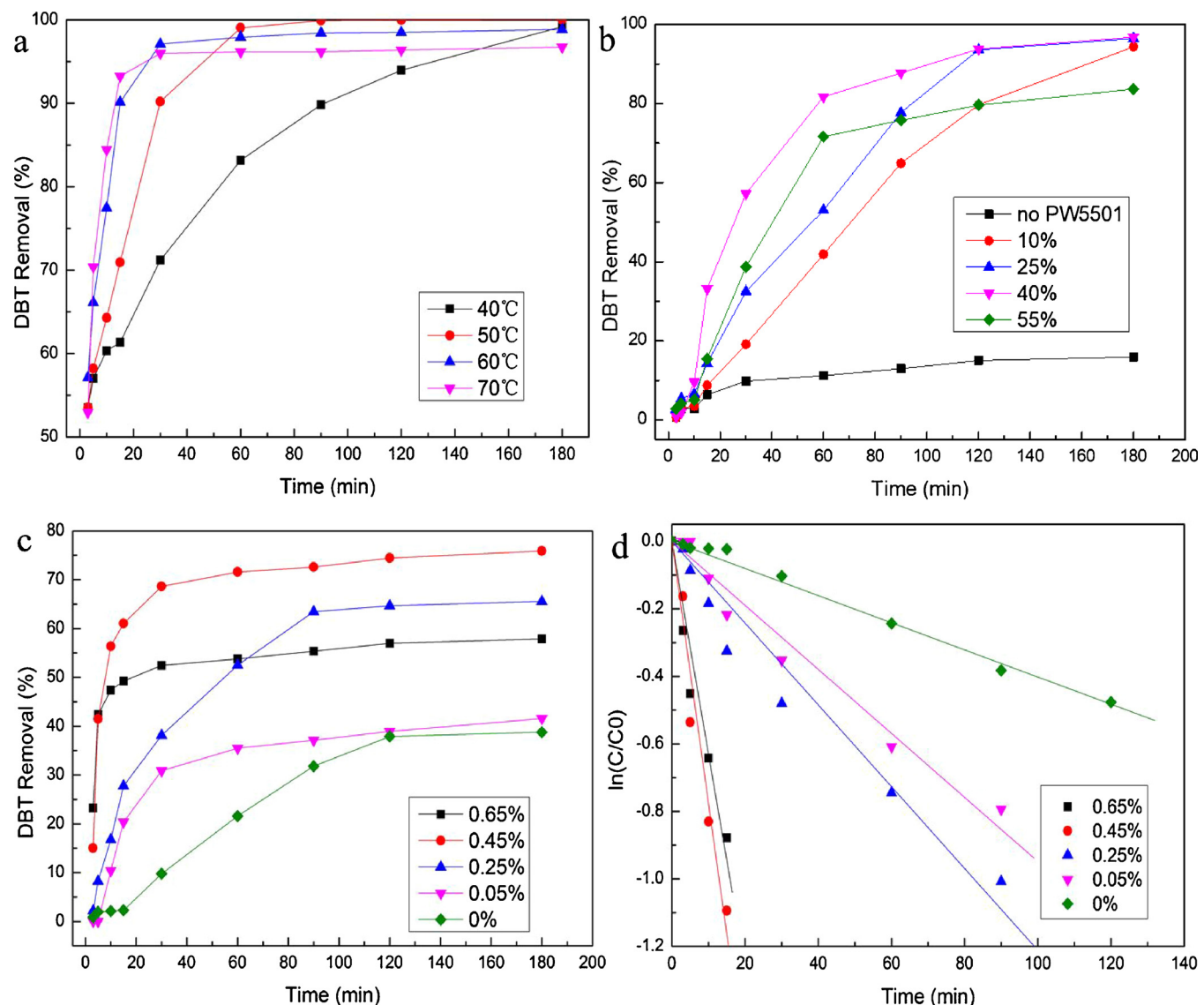


Fig. 9. Effect of reaction temperature (a), loading of QPW5501 (b), loading of C-dots (c) on the DBT removal using $\text{SiO}_2@\text{C-dots}/\text{QPW5501}$ as catalyst. (d) Pseudo first-order kinetic curves of C-dots loading influence shown in (c). Reaction conditions: initial S-content in model oil: 250 ppm; catalyst dosage: 0.2 g; reaction temperature: 50 °C; $n(\text{H}_2\text{O}_2)/n(\text{DBT}) = 2:1$ in (a) and (b), $n(\text{H}_2\text{O}_2)/n(\text{DBT}) = 1:1$ in (c); acetonitrile was used as extraction solvent in (a) and no extraction solvent was used in (b) and (c).

Table 2
Reaction rate constants k under different loading of C-dots.

C-dots loadings (%)	k (min^{-1})	R^2
0	0.0040	0.99
0.05	0.0094	0.98
0.25	0.0121	0.97
0.45	0.0777	0.98
0.65	0.0630	0.98

Table 3
Turn over frequencies (TOFs) of C-dots component on $\text{SiO}_2@\text{C-dots}/\text{QPW5501}$ with different C-dots loadings.

C-dots loadings (%)	Surface area (m^2/g)	TOF ($\text{mol min}^{-1} \text{atom}_{\text{C-dot}}^{-1}$)
0	7.3	\
0.05	7.8	0.140
0.25	30.2	0.139
0.45	182.3	0.071
0.65	163.7	0.075

greatly improved by the addition of C-dots, and when the C-dots loading reached 0.45 wt.% the highest value of k 0.777 min^{-1} was achieved which is nearly 20 times higher than the reaction constant when no C-dots was loaded. It indicates that C-dots played an important role on the desulfurization performance of $\text{SiO}_2@\text{C-dots}/\text{QPW5501}$ as a cocatalyst. We calculated the TOF values of the C-dots component in $\text{SiO}_2@\text{C-dots}/\text{QPW5501}$ catalyst with different C-dots loadings. TOF = number of transformed DBT per minute/ number of active sites. The number of active sites was approximated by the number of C-dot atoms in the catalyst. As shown in Table 3, TOFs of C-dots were very close when the loading of C-dots increased from 0.05% to 0.25%. However, the TOFs decreased significantly as the C-dots loading came to 0.45% and 0.65%. Surface areas data of different catalysts listed in Table 3 indicates that TOF values were related to the surface areas of the catalysts inversely. As we all know that large surface areas means low dispersity of the active sites, it can be suggested that closer proximity is beneficial to the intrinsic ODS activity of the C-dots in $\text{SiO}_2@\text{C-dots}/\text{QPW5501}$.

To further confirm the effect of C-dots in $\text{SiO}_2@\text{C-dots}/\text{QPW5501}$ /

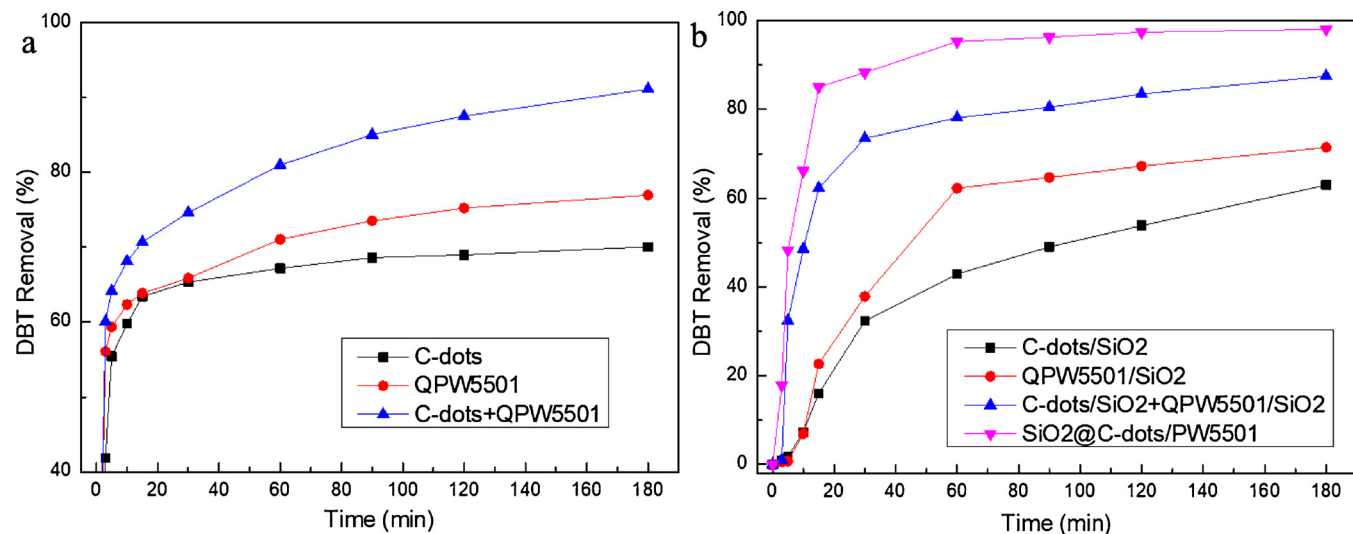


Fig. 10. (a) Oxidative desulfurization with C-dots and QPW5501, each one alone and both together. Reaction conditions: initial S-content in model oil: 50 ppm; C-dots dosage: 0.001 g, QPW5501 dosage: 0.05 g reaction temperature: 50 °C; $n(H_2O_2)/n(DBT) = 1.75:1$; extraction agent: 60 mL acetonitrile. (b) adsorptive-oxidative desulfurization with C-dots/SiO₂ and QPW5501/SiO₂, separately and together. Reaction conditions: initial S-content in model oil: 250 ppm; C-dots/SiO₂ dosage: 0.2 g, QPW5501/SiO₂ dosage: 0.2 g reaction temperature: 50 °C; $n(H_2O_2)/n(DBT) = 1.75:1$.

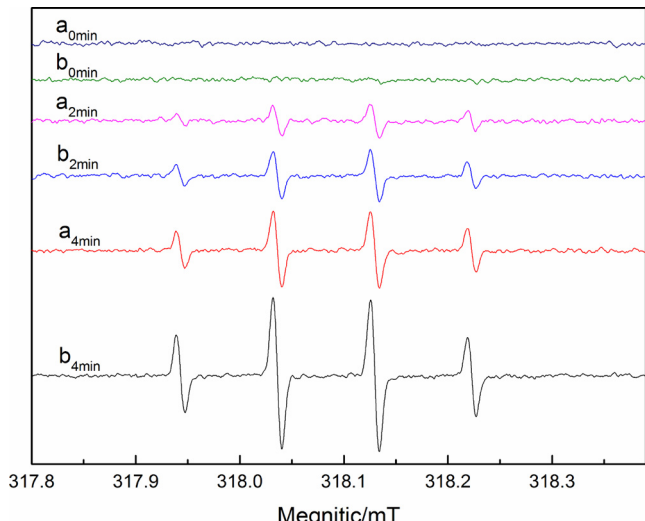


Fig. 11. 5,5-Dimethyl-pyrroline-oxide (DMPO) spin-trapping EPR spectra of aqueous solution in presence of (a) SiO₂@C-dots/QPW5501 (C-dots loading: 0.45%; 2 g/L) or (b) C-dots (0.2 g/L) with H₂O₂ (80 mM) and DMPO (50 mM).

H₂O₂ system, detection of hydroxyl radicals is carried out by EPR in Fig. 11 using 5,5-Dimethyl-pyrroline-oxide (DMPO) as the radical scavenger. A quartet of signals with relative intensities of 1:2:2:1 from the DMPO-OH[·] products were detected in both SiO₂@C-dots/QPW5501/H₂O₂ and C-dots/H₂O₂ systems, suggesting that the hydroxyl radicals were formed in the two catalytic reaction systems [42]. According to the peak intensity shown in Fig. 11, the concentration of ·OH in C-dots/H₂O₂ system is higher than that of SiO₂@C-dots/QPW5501/H₂O₂, and it might be caused by the fact that C-dots content in C-dots/H₂O₂ system (0.2 g/L) is higher than that in SiO₂@C-dots/QPW5501/H₂O₂ system (0.009 g/L) [43]. This also gives the evidence that the interaction between C-dots and H₂O₂ dominate the formation of ·OH. The higher reaction rate and enhanced DBT removal after C-dots was loaded on the catalyst can be attributed to the extremely high oxidative activity of ·OH. The catalytic activity of C-dots could be explained by the formation of a transition complex [C··H₂O₂], which can transfer the electron from the π-system to H₂O₂ molecule to generate ·OH during the decomposition process of H₂O₂ [33,44].

Table 4

DBT removal under different $n(H_2O_2)/n(DBT)$ on SiO₂@C-dots/QPW5501 and SiO₂@ QPW5501. Reaction conditions: initial S-content in model oil: 250 ppm; catalyst dosage: 0.2 g; reaction temperature: 50 °C; QPW5501 loading: 25%.

$n(H_2O_2)/n(DBT)$	DBT Removal after 180 min(%)	
	SiO ₂ @ C-dots/QPW5501 (C-dots loading 0.45%)	SiO ₂ @ QPW5501 (C-dots loading 0%)
0 (no H ₂ O ₂)	3.11	3.34
1:1	77.89	38.79
1.5:1	92.01	59.62
1.75:1	98.08	71.47
2:1	98.83	93.83
3:1	100	100

To figure out the mechanism of C-dots' catalytic effect, oxidation desulfurization experiments with C-dots and QPW5501 and oxidative-adsorptive desulfurization experiments with C-dots/SiO₂ (loading of PW5501 is 0) and PW5501/SiO₂ (loading of C-dots is 0) were carried out separately and together in Fig. 10. As shown in Fig. 10(a), DBT removal was about 70% and 76% after extraction with acetonitrile when the C-dots and QPW5501 was used as catalyst alone separately. Higher desulfurization efficiency was obtained when C-dots was used as catalyst alone compared with pure extraction desulfurization efficiency of 48.45%, which verified that C-dots could catalyze the oxidation of DBT with H₂O₂. That could be attributed to the ·OH species generated from the interaction between C-dots and H₂O₂. It was found that when C-dots and QPW5501 were used together in the system, the desulfurization efficiency was improved obviously. The similar improvement is also observed in Fig. 10(b) where the DBT removal was remarkably enhanced when the two catalysts C-dots/SiO₂ and PW5501/SiO₂ were used together than each one alone. Therefore, it can be suggested that besides oxidizing DBT straightly, the ·OH species produced by C-dots could also promote the oxidation of QPW5501 loaded on the catalyst to produce more catalytic active species {PO₄[WO(O₂)₂]₄}³⁻ in the solution. And the synergetic effect of C-dots and QPW5501 would lead to higher reaction rate and desulfurization efficiency. In addition, the synergetic effect of C-dots and QPW5501 would be stronger when the two components have closer proximity by being loaded on the same material according to Fig. 10(b). However, it should be noted that in Fig. 10(b), the DBT removal of C-dots/SiO₂ could reach 63% when n

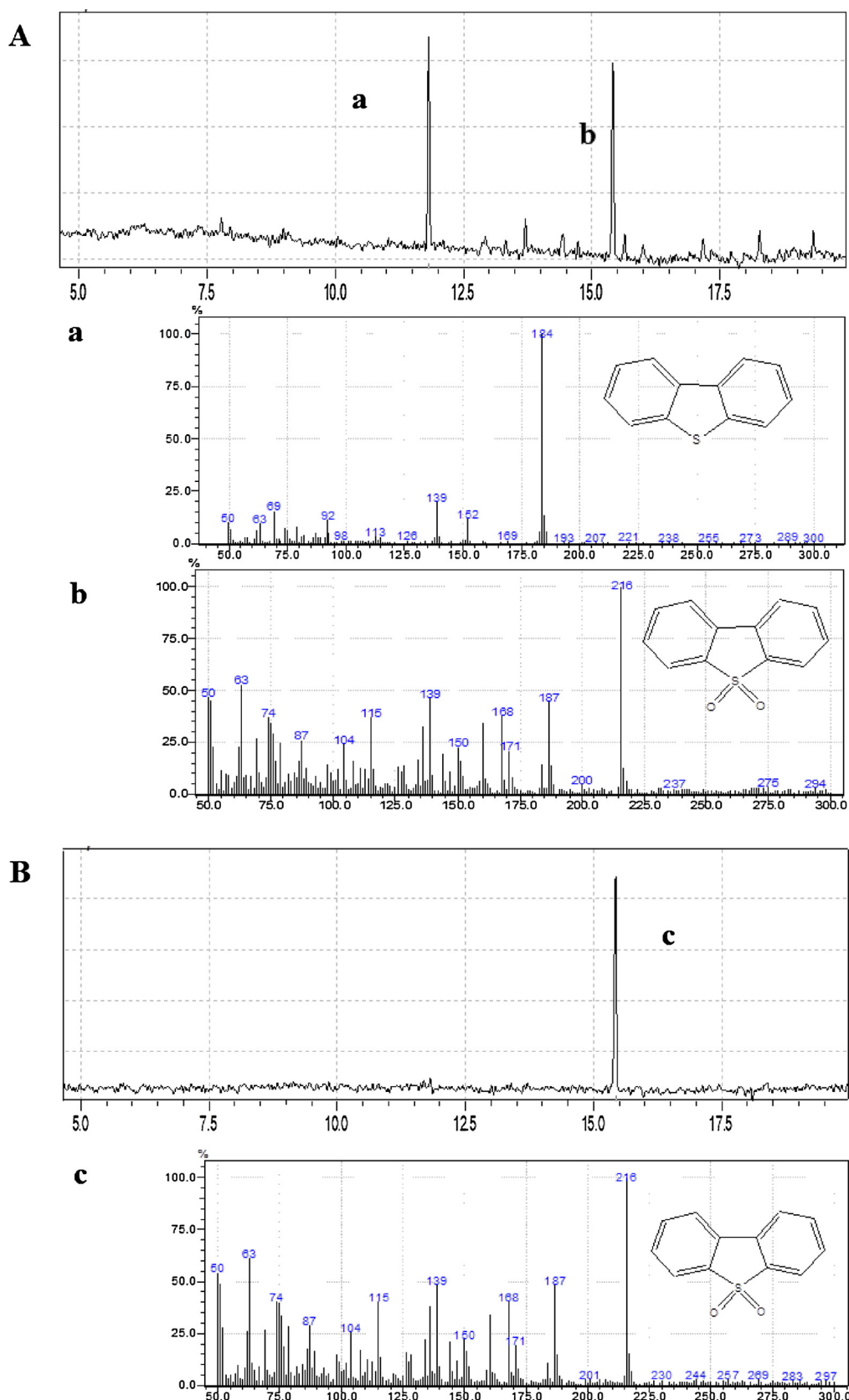


Fig. 12. GC-MS spectra of the oil phase after (A) 5 min and (B) 120 min in OADS system with $\text{SiO}_2@\text{C-dots}/\text{PW5501}$ as catalyst.

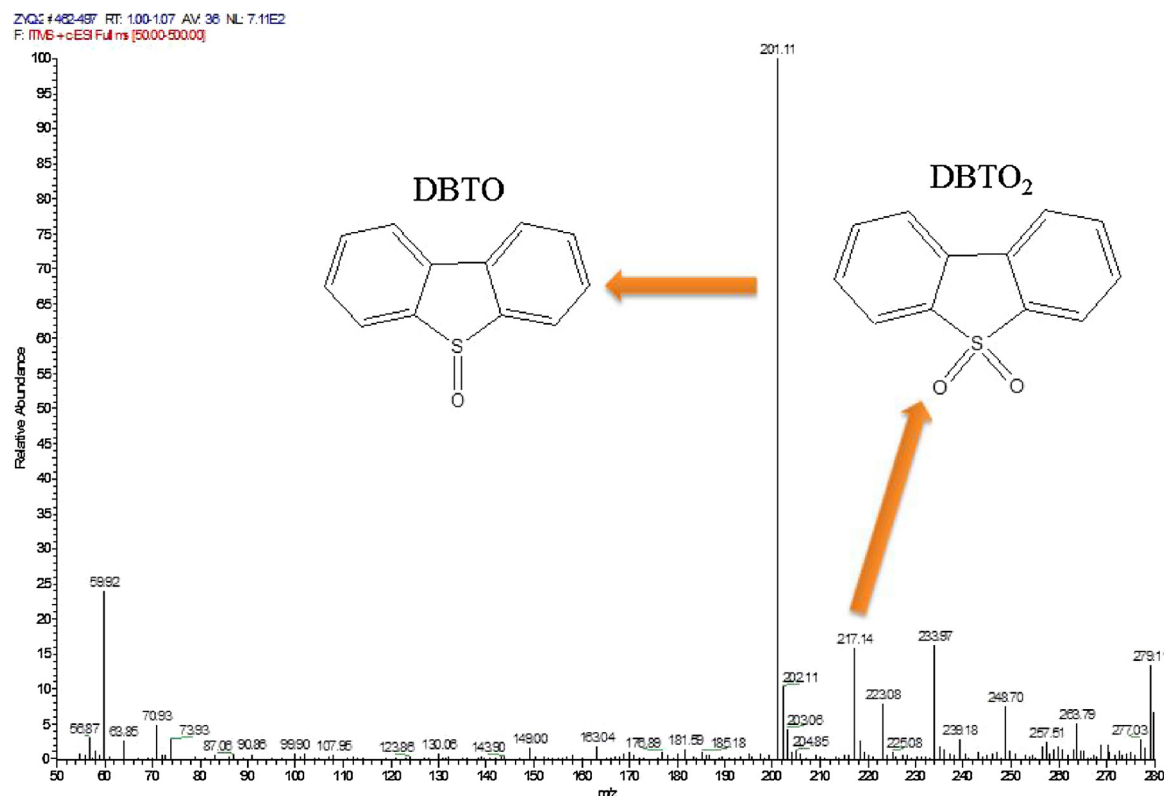


Fig. 13. LC-MS spectra of the acetonitrile eluent of the spent $\text{SiO}_2@\text{C-dots}/\text{QPW5501}$.

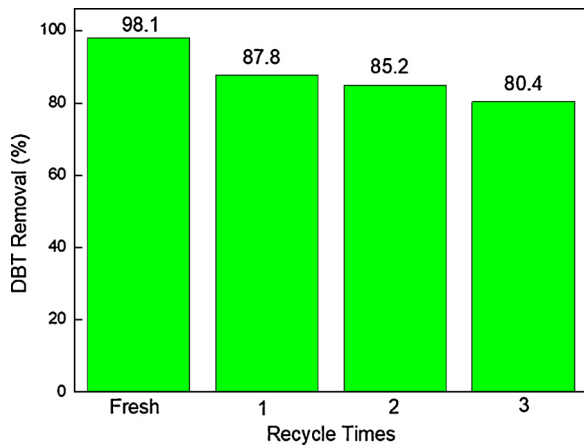


Fig. 14. OADS capacities of $\text{SiO}_2@\text{C-dots}/\text{QPW5501}$ at three constant regeneration cycles (conditions: initial S-content in model: 250 ppm; $n(\text{H}_2\text{O}_2)/n(\text{DBT}) = 1.75:1$; temperature: 50 °C; catalyst dosage: 0.2 g).

$(\text{H}_2\text{O}_2)/n(\text{DBT})$ is 1.75, while in Fig. 9(b), a much lower DBT removal of 16% was obtained with C-dots/ SiO_2 when $n(\text{H}_2\text{O}_2)/n(\text{DBT})$ is 2. This might because that more water phase introduced into the system with a higher dosage of H_2O_2 inhibited the contact between $\cdot\text{OH}$ in water phase and DBT in oil phase. The specific reason needs to be studied in the future.

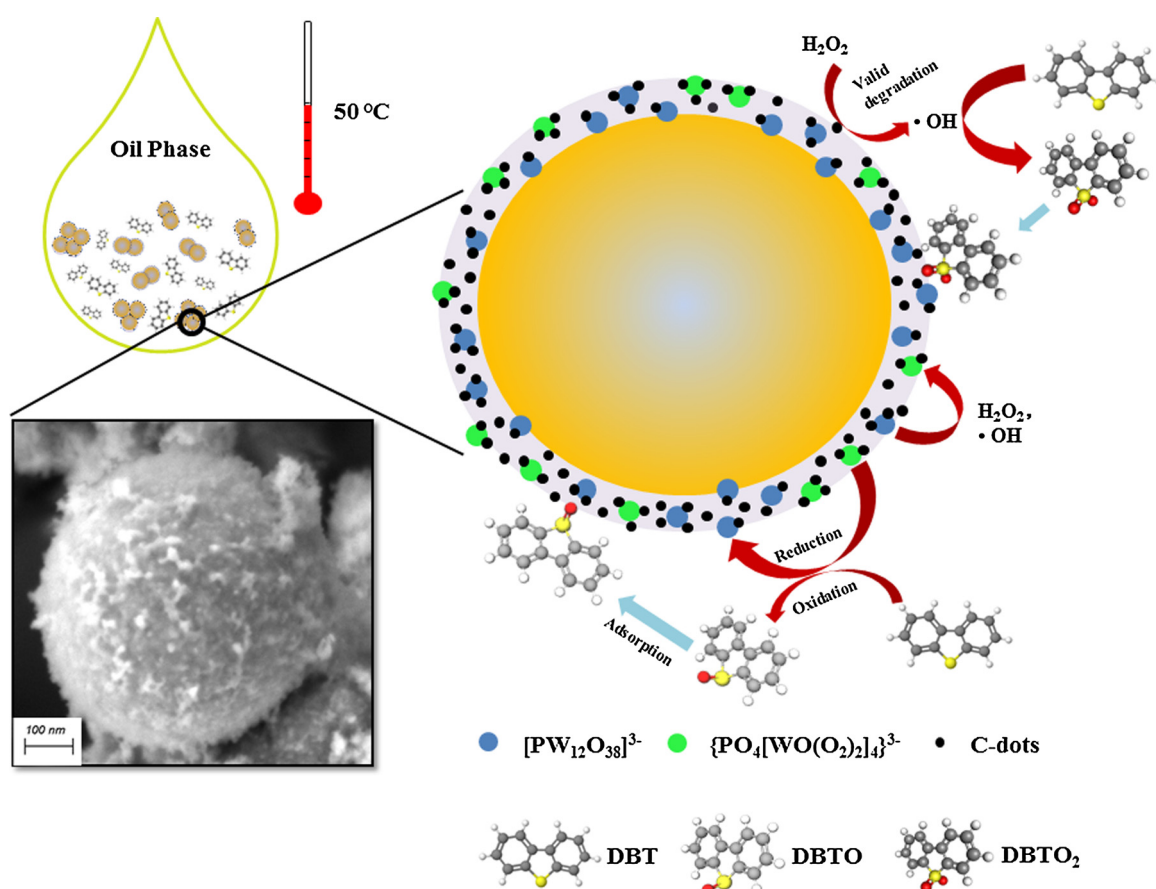
3.3.3. Effect of $n(\text{H}_2\text{O}_2)/n(\text{DBT})$

DBT removal of the OADS system under different $n(\text{H}_2\text{O}_2)/n(\text{DBT})$ on $\text{SiO}_2@\text{C-dots}/\text{QPW5501}$ and $\text{SiO}_2@\text{QPW5501}$ are presented in Table 4. As $n(\text{H}_2\text{O}_2)/n(\text{DBT})$ is increased, desulfurization efficiency for DBT was markedly enhanced, and the DBT in model fuel could be eliminated completely when the ratio of H_2O_2 and DBT reached 3. It also can be seen that, the desulfurization efficiency for DBT on $\text{SiO}_2@\text{C-dots}/\text{QPW5501}$

(C-dots loading 0.45%) is much higher than that on $\text{SiO}_2@\text{QPW5501}$ under the same ratio of H_2O_2 and DBT. That gives the evidence that the participation of C-dots in the reaction could enhance the utilization of H_2O_2 . It is noteworthy that a high desulfurization efficiency of 98.08% could be achieved even when $n(\text{H}_2\text{O}_2)/n(\text{DBT})$ was as low as 1.75. As we all know, the stoichiometric amount of H_2O_2 for converting DBT to its corresponding sulfone (DBTO₂) completely is twice molar amount of DBT. According to our former work, the other oxidized product of DBT sulfoxide (DBTO) which needs less oxidant in its conversion could also be removed effectively from the oil phase by adsorption [45]. Therefore, it can be concluded that part of DBT in $\text{SiO}_2@\text{C-dots}/\text{QPW5501}/\text{H}_2\text{O}_2$ OADS system was oxidized to DBTO and removed at this form by adsorption on the $\text{SiO}_2@\text{C-dots}/\text{QPW5501}$.

3.4. OADS mechanism in $\text{SiO}_2@\text{C-dots}/\text{QPW5501}/\text{H}_2\text{O}_2$ system

The oxidation process of DBT in OADS system was studied by GC-MS spectrum. As shown in Fig. 12(A), two main compounds ascribed to DBT and DBTO₂ were detected when the reaction time was 5 min. When the reaction time reached 120 min, only one compound was detected in Fig. 12(B) which was assigned to DBTO₂. It indicates that, DBT can be oxidized to its corresponding sulfone completely by catalyst and oxidant in OADS system. But the peaks of DBTO and DBTO₂ were overlapped severely and only DBTO₂ could be identified on the GC-MS spectra. Therefore, LC-MS spectra of the acetonitrile eluent of spent $\text{SiO}_2@\text{C-dots}/\text{QPW5501}$ were also carried out to detect the sulfur species adsorbed on the catalyst after reaction. As shown in Fig. 13, the peak at m/z 201.11 and m/z 217.14 can identify the existence of DBTO and DBTO₂, which means that both DBTO and DBTO₂ were produced from the oxidation conversion of DBT and the two oxidized products can be adsorbed efficiently on $\text{SiO}_2@\text{C-dots}/\text{QPW5501}$ in the OADS process. From the reuse experiments results shown in Fig. 14, it can be seen that the desulfurization efficiency decreased from 98.1% to 80.4% after 3 times recycles. BET surface area of spent $\text{SiO}_2@\text{C-dots}/\text{QPW5501}$ was characterized to be $235.12 \text{ m}^2\text{g}^{-1}$ which is much higher



Scheme 2. Schematic description of the mechanism for the OADS process with $\text{SiO}_2@\text{C-dots}/\text{QPW5501}$ catalyst and H_2O_2 .

than that of fresh $\text{SiO}_2@\text{C-dots}/\text{QPW5501}$ (109.5). Therefore, the loss of the desulfurization capacity was mainly caused by the resume of high active $[\text{PW}_{12}\text{O}_{38}]^{3-}$ back to low active $[\text{PW}_{12}\text{O}_{40}]^{3-}$ after oxidation reaction which have been confirmed by XRD spectrum in Fig. 1(c).

According to the results obtained above, a schematic description of mechanism for the desulfurization process in $\text{SiO}_2@\text{C-dots}/\text{QPW5501}/\text{H}_2\text{O}_2$ OADS system is proposed in Scheme 2. QPW5501 in the shell improves the compatibility of the catalyst surface with the oil phase which is beneficial for the mass transfer in the heterogeneous system [17,18]. The high specific surface area supplied by the microsphere structure of the catalyst provides the maximum accessibility for the catalytic active sites dispersed in the external shell. Furthermore, the oxidant H_2O_2 can be effectively utilized in two different paths for the oxidation of DBT in this system. First, H_2O_2 can react with heteropolyanions $[\text{PW}_{12}\text{O}_{38}]^{3-}$ to produce high active peroxoheteropolyanions $\{\text{PO}_4[\text{WO}(\text{O}_2)_2]_4\}^{3-}$, and which plays a leading role for the oxidation of DBT in normal Keggin POMs/ H_2O_2 systems. Meanwhile, H_2O_2 could also be effectively utilized via the interaction with the co-catalyst C-dots to generate hydroxyl radicals in this system, and the produced $\cdot\text{OH}$ could participate in the oxidation of DBT directly or help convert $[\text{PW}_{12}\text{O}_{38}]^{3-}$ to $\{\text{PO}_4[\text{WO}(\text{O}_2)_2]_4\}^{3-}$ due to its high oxidative activity. After the DBT was oxidized, the sulfoxides and sulfones converted from the oxidation of DBT were adsorbed on the catalyst subsequently, and the sulfur compounds are eliminated from the oil by the separation of the solid catalyst. The synergistic effect of the core-shell microsphere structure, highly active $[\text{PW}_{12}\text{O}_{38}]^{3-}$ in QPW5501 and the cocatalyst C-dots provides high adsorptive ability and high catalytic activity for the catalyst simultaneously, which is responsible for the high desulfurization efficiency of the OADS system.

4. Conclusion

The mesoporous core-shell microsphere catalyst $\text{SiO}_2@\text{C-dots}/\text{QPW5501}$ was successfully synthesized and employed as both catalyst and adsorbent for OADS of the refractory organic sulfur compound DBT in oil phase with aqueous H_2O_2 . High desulfurization efficiency of 98.08% could be accomplished with a lower ratio of $\text{H}_2\text{O}_2/\text{DBT}$ as 1.75 which is less than the stoichiometric amount of H_2O_2 . The activity of HPW loaded on the catalyst was found to be greatly enhanced by calcination at 550 °C for 1 h due to formation of the defective Keggin structure $[\text{PW}_{12}\text{O}_{38}]^{3-}$. The temperature and time of thermal treatment prove to be crucial for the activity enhancement. C-dots showed unprecedented catalytic effect in this H_2O_2 oxidized reaction as a promoter in the catalyst. H_2O_2 can be effective decomposed by the interaction with C-dots to produce $\cdot\text{OH}$ which owns extraordinary oxidative activity. The additional path supplied by C-dots for the utilization of H_2O_2 played a vital role to the decline of the invalid degradation of H_2O_2 . In summary, the synergistic effect of the unique structure of the catalyst, highly active phosphotungstate after calcination and the co-catalyst C-dots ensures the good performance of $\text{SiO}_2@\text{C-dots}/\text{QPW5501}$ in OADS system with less oxidant.

Acknowledgments

Thanks for the financial support by National Natural Science Foundation of China (21076116; 21511130021) and PetroChina Innovation Foundation (2010D-5006-0405).

References

[1] B. Bertleff, J. Claußnitzer, W. Korth, P. Wasserscheid, A. Jess, J. Albert, ACS

Sustain. Chem. Eng. 5.5 (2017) 4110–4118.

[2] D. Piccinino, I. Abdalghani, G. Botta, M. Crucianelli, M. Passacantando, M.L.D. Vacri, R. Saladino, Appl. Catal. B 200 (2017) 392–401.

[3] J.T. Sampantar, H. Xiao, J. Dou, T.Y. Nah, X. Rong, W.P. Kwan, Appl. Catal. B 63 (2006) 85–93.

[4] C. Song, X. Ma, Appl. Catal. B 41 (2003) 207–238.

[5] H. Yang, B. Jiang, Y. Sun, L. Zhang, Z. Huang, Z. Sun, N. Yang, J. Hazard. Mater. 333 (2017) 63–72.

[6] F. Al-Shahrani, T. Xiao, S.A. Llewellyn, S. Barri, Z. Jiang, H. Shi, G. Martinie, M.L.H. Green, Appl. Catal. B 73 (2007) 311–316.

[7] W. Zhu, G. Zhu, H. Li, Y. Chao, M. Zhang, D. Du, Q. Wang, Z. Zhao, Fuel Process. Technol 106 (2013) 70–76.

[8] Q. Gu, G. Wen, Y. Ding, K.H. Wu, C. Chen, D. Su, Green. Chem. 19 (2017) 1175–1181.

[9] C. Jiang, J. Wang, S. Wang, H. Guan, X. Wang, M. Huo, Appl. Catal. B 106 (2011) 343–349.

[10] Y. Zhang, D. Li, Y. Chen, X. Wang, S. Wang, Appl. Catal. B 86 (2009) 182–189.

[11] S. Liu, L. Chen, G. Wang, J. Liu, Y. Gao, C. Li, H. Shan, J. Energy. Chem. 25 (2016) 85–92.

[12] X.S. Wang, L. Li, J. Liang, Y.B. Huang, R. Cao, ChemCatChem 9 (2017) 971–979.

[13] H. Lü, W. Ren, W. Liao, W. Chen, Y. Li, Z. Suo, Appl. Catal. B 138–139 (2013) 79–83.

[14] H. Lü, W. Ren, H. Wang, Y. Wang, W. Chen, Z. Suo, Appl. Catal. A 453 (2013) 376–382.

[15] J. Xiong, W. Zhu, W. Ding, L. Yang, Y. Chao, H. Li, F. Zhu, H. Li, Ind. Eng. Chem. Res. 53 (51) (2014) 19895–19904.

[16] Á. Kukovecz, Z. Balogi, Z. Kónya, M. Tobab, P. Lentz, S.I. Niwa, F. Mizukamib, Á. Molnár, J.B. Nagy, I. Kiricsi, Appl. Catal. A 228 (2002) 83–94.

[17] J.W. Ding, R. Wang, Chin. Chem. Lett. 27 (2016) 655–658.

[18] R. Liu, Y. Zhang, J. Ding, R. Wang, M. Yu, Sep. Purif. Technol. 174 (2017) 84–88.

[19] R. Wang, F. Yu, G. Zhang, H. Zhao, Catal. Today 150 (2010) 37–41.

[20] F. Liu, L. Wang, Q. Sun, L. Zhu, X. Meng, F.S. Xiao, J. Am. Chem. Soc. 134 (2012) 16948–16950.

[21] B. Karimi, M. Khorasani, ACS Catal. 3 (2013) 1657–1664.

[22] S. Xun, W. Zhu, F. Zhu, Y. Chang, D. Zheng, Y. Qin, M. Zhang, W. Jiang, H. Li, Chem. Eng. J. 280 (2015) 256–264.

[23] M. Zhang, W. Zhu, H. Li, S. Xun, W. Ding, J. Liu, Z. Zhao, Q. Wang, Chem. Eng. J. 243 (2014) 386–393.

[24] Qi. Gu, W. Zhu, S. Xun, Y. Chang, J. Xiong, M. Zhang, W. Jiang, F. Zhu, H. Li, Fuel 117 (2014) 667–673.

[25] L. Hao, M. Wang, W. Shan, C. Deng, W. Ren, Z. Shi, H. Lü, J. Hazard. Mater. 339 (2017) 216–222.

[26] R. Zhao, J. Wang, D. Zhang, Y. Sun, B. Han, N. Tang, J. Zhao, K. Li, A.C.S. Sustain. Chem. Eng. 5 (2017) 2050–2055.

[27] J.M. Fraile, C. Gil, J.A. Mayoral, B. Muel, L. Roldán, E. Vispe, S. Calderón, F. Puente, Appl. Catal. B 180 (2016) 680–686.

[28] L. Zhang, J. Wang, Y. Sun, B. Jiang, H. Yang, Chem. Eng. J. 8 (2017) 445–453.

[29] Y. Hu, Q. He, Z. Zhang, N. Ding, B. Hu, Chem. Commun. 47 (2011) 12194–12196.

[30] C. Li, Z. Jiang, J. Gao, Y. Yang, S. Wang, F. Tian, F. Sun, X. Sun, P. Ying, C. Han, Chem. Eur. J. 10 (2004) 2277–2280.

[31] J. Liu, Y. Liu, N. Liu, Y. Han, X. Zhang, H. Huang, Y. Lifshitz, S.T. Lee, J. Zhong, Z. Kang, Science 347 (6225) (2015) 970–974.

[32] Q. Du, W. Wang, Y. Wu, G. Zhao, F. Ma, X. Hao, RSC Adv. 5 (2015) 31057–31063.

[33] H. Ming, Z. Ma, Y. Liu, K. Pan, H. Yu, F. Wang, Z. Kang, Dalton Trans. 41 (2012) 9526–9531.

[34] D.S. Su, S. Perathoner, G. Centi, Chem. Rev. 113 (2013) 5782–5816.

[35] U.B. Mioč, R.Ž. Dimitrijević, M. Davidović, Z.P. Nedić, M.M. Mitrović, P.H. Colombar, J. Mater. Sci. 29 (1994) 3705–3718.

[36] X.M. Yan, P. Mei, J. Lei, Y. Mi, L. Xiong, L. Guo, J. Mol. Catal. A: Chem. 304 (2009) 52–57.

[37] S. Cong, Y. Tian, Q. Li, Z. Zhao, F. Geng, Adv. Mater. 26 (2014) 4260–4267.

[38] S. Zhang, G. Zhaoa, S. Gao, Z. Xia, J. Xua, J. Mol. Catal. A: Chem. 289 (2008) 22–27.

[39] L. Salles, J.Y. Piquemal, R. Thouvenot, C. Minot, J.M. Brkgeault, J. Mol. Catal. A: Chem. 117 (1997) 375–387.

[40] L. Hua, Y.X. Qiao, H. Li, B. Feng, Z.Y. Pan, Y.Y. Yu, Sci. China. Chem. 54 (2011) 769–773.

[41] M. Wang, X. Wang, Q. Yue, Y. Zhang, C. Wang, J. Chen, H. Cai, H. Lu, A.A. Elzatahry, D. Zhao, Y. Deng, Chem. Mater. 26 (2014) 3316–3321.

[42] Yu. Yao, L. Wang, L. Sun, S. Zhu, Z. Huang, Y. Mao, W. Lu, W. Chen, Chem. Eng. Sci. 101 (2013) 424–431.

[43] T. Wen, W. He, Y. Chong, Y. Liu, J.J. Yin, X. Wu, Phys. Chem. Chem. Phys. 17 (2015) 24937–24943.

[44] V.F. Lapko, I.P. Gerasimyuk, V.S. Kuts', Y.A. Tarasenko, Russ. J. Phys. Chem. A 84 (6) (2010) 934–940.

[45] Y. Zhang, R. Wang, Diam. Relat. Mater. 73 (2017) 161–168.